JOURNAL OF SOLID STATE CHEMISTRY **125,** 85–90 (1996)
ARTICLE NO. 0268

Subsolidus Phase Relations in $BiO_{3/2}$–$PrO_{11/6}$–CuO

Yang Jinling,*,[1] Liang Jingkui,*,† Tang Weihua,* Shi Ying,* Chen Xiaolong,* and Rao Guanghui*

*Institute of Physics, Chinese Academy of Sciences, Beijing 100080, People's Republic of China; and †International Center for Materials Physics, Academia Sinica, Shenyang 110015, People's Republic of China

Received July 26, 1995; in revised form April 9, 1996; accepted May 15, 1996

The subsolidus phase relations in the $BiO_{3/2}$–$PrO_{11/6}$–CuO ternary oxide system and in the related binary systems as well as crystallographic parameters of selected phases are investigated by X-ray powder diffraction. The subsolidus phase relation at room temperature in the $BiO_{3/2}$–$PrO_{11/6}$–CuO system can be divided into three two-phase regions and five three-phase regions. No ternary compound was found. There exist two solid solutions $(BiO_{3/2})_{1-x}(PrO_{11/6})_x$ in the $BiO_{3/2}$–$PrO_{11/6}$ system with $x = 0.1$–0.3 and $x = 0.69$–0.72, respectively. Both belong to the rhombohedral system ($R\bar{3}m$). The lattice parameters represented by a hexagonal cell are $a = 3.9986(7)$ Å, $c = 27.459(6)$ Å for Bi_3PrO_y (α phase) and $a = 3.8729(5)$ Å, $c = 9.7452(2)$ Å for $Bi_3Pr_7O_y$ (γ phase). The Rietveld refinement result of the crystal structure of $Bi_3Pr_7O_y$ reveals that Bi/Pr atoms occupy statistically the 3*a* site and O atoms and vacancies occupy the 6*c* site. Pr^{3+} is the major state in the two solid solutions.

INTRODUCTION

The crystal structures of high T_c oxide superconductors are closely related to the perovskite-type structure ($RCuO_{3-\delta}$) formed by the rare earth and copper oxides. $RCuO_{3-\delta}$ block layers and Bi_2O_2 block layers stack alternatively to form a series of compounds of the general formula $(Bi_2O_2)_n(RCuO_{3-\delta})_m$. In addition, Bi^{3+} has a lone pair of electrons outside its filled *d* shell, which can form bonds with neighboring coordination oxygen ions and cause distortion of the coordination polyhedra. Therefore, structures with polarization or without center of symmetry would be formed, for example, the known ferroelectronics $Bi_4Ti_3O_{12}$ and $BiWO_3$. Based on the above two points, it is expected that in the system $BiO_{3/2}$–$RO_{3/2}$–CuO, there could be some compounds with layered perovskite-type structures, incommensurated structures, or structures without center of symmetry. From the structural point of view, these compounds could be potential high T_c oxide superconductors and ferroelectrics. It is well known that phase diagrams play an important role in explaining the relationship of composition, structure, and property, and also in optimizing synthesis conditions. However, the phase diagrams of $BiO_{3/2}$–$RO_{3/2}$–CuO ternary systems were not properly explored. In this paper, we have conducted investigations on the subsolidus phase relations in the $BiO_{3/2}$–$PrO_{11/6}$–CuO ternary system and in its binary systems.

EXPERIMENTAL DETAILS

Samples were prepared by the solid state reaction method using analytically pure Bi_2O_3, Pr_6O_{11}, and CuO as starting materials. Stoichiometric amounts of starting materials were appropriately weighed, mixed, and ground in an agate mortar. The well-mixed powder was pressed into pellets of 10–12 mm in diameter and 1–2 mm in thickness, and then were sintered in air for 4 days. The phase components of the samples remained unchanged on long-time sintering, which indicated that the samples were in their equilibrium states. Due to the low melting point (825°C) of Bi_2O_3, the Bi_2O_3-poor samples (<50 mol% Bi_2O_3) were sintered at 850°C, while other samples were sintered at 750°C. All samples were cooled in a furnace to room temperature.

Phase identification and structure analysis were performed using a Guinier–de Wolf monochromatic focusing transmission camera and a M18AHF X-ray diffractometer with Cu$K\alpha$ radiation (50 kV × 200 mA) and graphitic monochromator, respectively. The lattice parameters were refined using a standard least-squares method. Pure Si powder was used as internal standard.

RESULT AND DISCUSSION

Binary System

In the binary system $PrO_{11/6}$–CuO, only one compound, Pr_2CuO_4, was obtained, which is consistent with the results of Hodorowicz *et al.* (1). It belongs to the tetragonal lattice, space group $I4/mmm$, with lattice parameters $a = 3.960$ Å and $c = 12.230$ Å. Pr_2CuO_4 is a semiconductor.

[1] To whom correspondence should be addressed.

0022-4596/96 $18.00

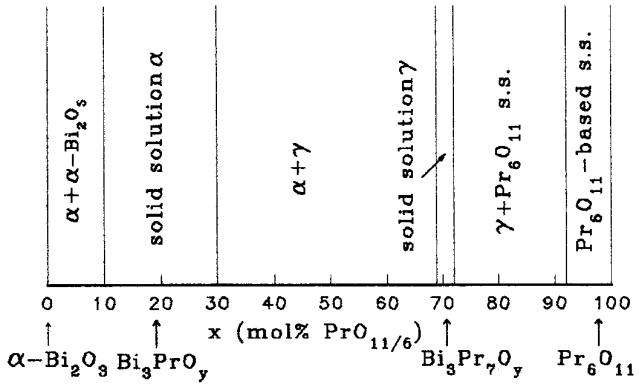

FIG. 1. Subsolidus phase relations in the Bi_2O_3–Pr_6O_{11} binary system.

In the binary system $BiO_{3/2}$–CuO, there also exists only one compound, Bi_2CuO_4. The result we obtained is very close to that obtained by Boivin *et al.* (2). The compound crystallizes in the tetragonal lattice with $a = 8.150$ Å and $c = 5.814$ Å and space group $P4/ncc$.

The isothermal section of the subsolidus phase relation at room temperature in the $BiO_{3/2}$–$PrO_{11/6}$ system is shown in Fig. 1. The representative X-ray diffraction patterns of the annealed $(BiO_{3/2})_{1-x}(PrO_{11/6})_x$ are shown in Fig. 2. Pure Bi_2O_3 belongs to the monoclinic system and pure Pr_6O_{11} to the fluorite-like fcc structure. The samples with $x = 0.1$–0.3 and $x = 0.69$–0.72 crystallize in two rhombohedral phases, which have the same space group $R\bar{3}m$, but different crystal structures. Each phase has a certain solubility. Herafter, we identify these rhombohedral phases as solid solution α and solid solution γ. The solid solution α corresponds to the β phase in the Bi_2O_3–SrO system studied by Sillen and Aurivillius (3) and Boivinet *et al.* (4). Judging from the diffraction pattern, the solid solution γ may be considered as being derived from a distorted fcc structure (5, 6).

The solid solution range of $PrO_{11/6}$ in $BiO_{3/2}$ is very limited; the samples with $x = 0.02$ comprised Bi_2O_3 and solid solution α. It is estimated that the solid solution limit is lower than 0.02. The result is consistent with the fact that, in the phase diagram of Bi_2O_3-rich region of the $(Bi_2O_3)_{1-x}(Sm_2O_3)_x$ system (7), the solid solution limit of Sm_2O_3 in Bi_2O_3 is lower than 0.005.

For the terminal solid solution based on the Pr_6O_{11} matrix, there is no remarkable shift of the diffraction lines of the samples with different composition, which might be due to the small difference in the ionic radius of Bi^{3+} and Pr^{3+} and to the small content of Bi_2O_3. However, when the sample with $x = 0.92$ was mixed with pure Pr_6O_{11} in the volume ratio of 1 : 1, the small broadening and shift of reflection lines of the mixed sample, in comparison with those of pure Pr_6O_{11}, was observed (see inset in Fig. 2). In addition, the XRD pattern of the sample with $x = 0.92$ is similar to that of pure Pr_6O_{11} and does not show any trace of other phase. These results suggest that there exist Pr_6O_{11}-based solid solution and the solid solution range of $BiO_{3/2}$ in $PrO_{11/6}$ is wider ($x = 0.92$–1.0) than that of $PrO_{11/6}$ in $BiO_{3/2}$.

Solid solution α is a good oxide ionic conductor; its structure and conductivity have been studied by many researchers (8–10). It can be synthesized using different rare earth R_2O_3 oxides. In light of ionic radius of lanthanide elements, Iwahara *et al.* (8) deduced that the crystal structure of the system Bi_2O_3–R_2O_3 varied as the atomic numbers changed, from the rhombohedral phase for relatively large ionic radii of R^{3+} to fcc in the case of comparatively small radii of R^{3+}; the compound having a R^{3+} cation radius of medium size may be anticipated to contain both fcc

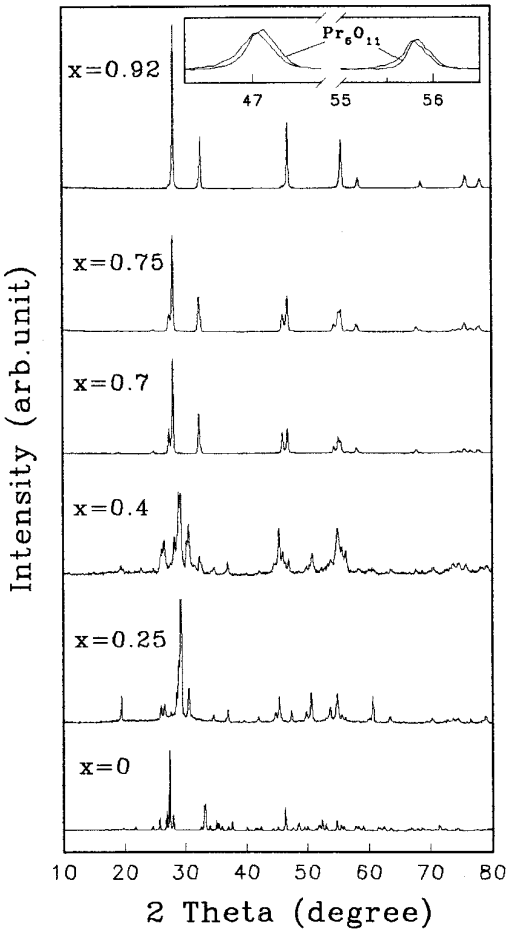

FIG. 2. X-ray powder diffraction patterns of $(BiO_{3/2})_{1-x}(PrO_{11/6})_x$ calcined in air for 4 days at 750°C for $x = 0$, 0.25, 0.4, and 850°C for $x = 0.7$, 0.75, 0.92, respectively. The inset shows the selected diffraction peaks (220) and (311) of the mixed sample ($x = 0.92$ and $x = 1.0$) and pure Pr_6O_{11}.

TABLE 1
List of *d* Spacings, Relative Intensities, and Miller Indices for Bi_3PrO_y, $a = 3.9986$ Å and $c = 27.459$ Å and Space Group $R\bar{3}m$

h k l	d_{obs} (Å)	d_{cal} (Å)	I_{rel}	*h k l*	d_{obs} (Å)	d_{cal} (Å)	I_{rel}
0 0 6	4.5623	4.5767	7	2 0 1	1.7269	1.7281	<1
1 0 1	3.4293	3.4358	4	1 0 14	1.706	1.7067	<1
1 0 2	3.3507	3.3578	4	1 1 9	1.6721	1.6723	5
1 0 4	3.0994	3.0919	12	2 0 5	1.6505	1.6514	2
0 0 9	3.0476	3.0511	100	0 0 18	1.5258	1.5256	7
1 0 5	2.9246	2.9293	11	1 0 17	1.4642	1.4639	2
1 0 7	2.5945	2.5961	2	2 0 11	1.4223	1.4228	<1
1 0 8	2.4352	2.4378	4	1 1 15	1.3497	1.3502	<1
1 0 10	2.1504	2.1516	2	2 0 13	1.3389	1.3391	2
1 0 11	2.0239	2.0239	3	2 0 14	1.2993	1.2981	<1
1 1 0	1.9976	1.9993	8	2 1 4	1.2859	1.2857	1
0 0 15	1.8301	1.8307	3	2 1 5	1.2734	1.2732	1
1 0 13	1.8031	1.8033	11	1 1 18	1.2133	1.2128	3

and rhombohedral phases, depending on composition. This inference has been verified experimentally. In our experiment, the rhombohedral phase occurred in the Bi_2O_3–Pr_6O_{11} system due to the large ionic radius of Pr^{3+}, which is also consistent with the reference.

Solid solution α is a phase stable at low temperature. The DTA measurement of the samples with $x = 0.1$–0.3 sintered at 750°C for 4 days showed a remarkable endothermic peak at 670–700°C during heating, but no thermal effect was observed on cooling. This endothermic peak corresponds to the transition from the rhombohedral phase to the fcc structure. The result was analogous to that of Watanabe *et al.* (10, 11) for Bi_2O_3–Ho_2O_3 and Bi_2O_3–Y_2O_3. They further annealed the synthesized fcc specimen at 650°C over 150 h and found that the fcc phase fully changed into the rhombohedral phase. They concluded that the transition from the rhombohedral phase into the fcc one is reversible, and that the transition during heating is much more rapid than that in the cooling process.

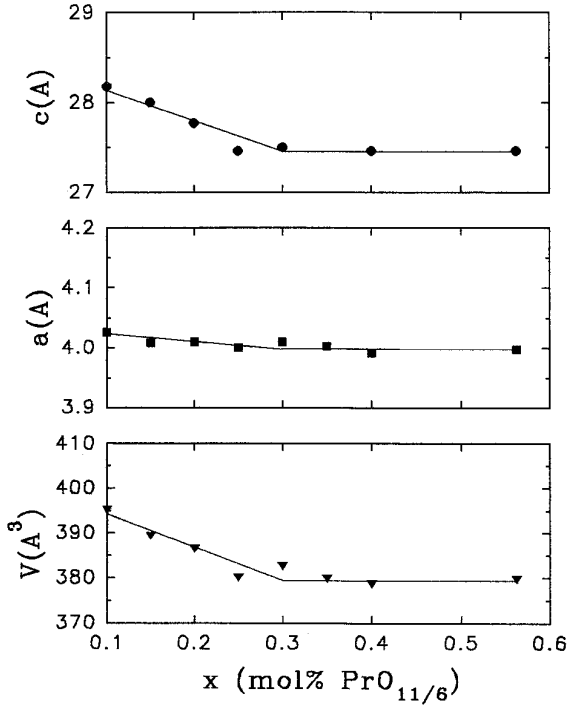

FIG. 3. The variation of lattice parameters a, c and V vs x in $(BiO_{3/2})_{1-x}(PrO_{11/6})_x$ with $x \leq 0.6$.

The diffraction lines of samples with $x = 0.25$ (Bi_3PrO_y) were indexed by using Werner's TREOR program (12). The indexing results of Bi_3PrO_y are listed in Table 1. It can be seen that all diffraction lines were indexed. The calculated spacings d_{cal} coincide well with those observed d_{obs}. The high de Wolff figure of merit (13), $M = 15$, indicates that the result of indexing is reliable. The indexing result of Bi_3PrO_y is close to that of $Bi_{1.55}Y_{0.45}O_3$ reported by Watanabe *et al.* (10). Bi_3PrO_y belongs to the rhombohedral system with lattice parameters $a = 3.9986(7)$ Å and $c = 27.459(6)$ Å in a hexagonal setting.

The variation of lattice parameters vs the $PrO_{11/6}$ content for solid solution α is shown in Fig. 3. The lattice parameter

TABLE 2
List of the Lattice Parameters and Cell Volumes of the Solid Solution γ Phase

Pr content	a (Å)	c (Å)	V (Å)
0.69	3.8750	9.7490	126.77
0.7	3.8729	9.7452	126.60
0.71	3.8748	9.7581	126.87

TABLE 3
List of *d* Spacings, Relative Intensities, and Miller Indices for the Fundamental Structure with $a = 3.8729$ Å and $c = 9.7452$ Å and Space Group $R\bar{3}m$ and the Superstructure Cell with $a = 30.983$ Å and $c = 19.490$ Å for $Bi_3Pr_7O_y$

$(h\ k\ l)_{sup}$	$(h\ k\ l)_f$	d_{obs} (Å)	d_{cal} (Å)	I_{obs}	$(h\ k\ l)_{sup}$	$(h\ k\ l)_f$	d_{obs} (Å)	d_{cal} (Å)	I_{obs}
1 1 4		4.6332	4.6341	1	16 0 2	2 0 1	1.6532	1.6527	13
5 2 3		3.5786	3.5794	3	0 0 12	0 0 6	1.6242	1.6242	2
0 0 6	0 0 3	3.2477	3.2484	30	16 0 4	2 0 2	1.5863	1.5857	6
8 0 2	1 0 1	3.1729	3.1714	100	16 0 8	2 0 4	1.3814	1.3814	4
8 0 4	1 0 2	2.7628	2.7626	42	8 8 10		1.3679	1.3678	2
8 0 8	1 0 4	1.9706	1.9712	21	8 0 14	1 0 7	1.2859	1.2858	2
8 8 0	1 1 0	1.9372	1.9365	26	16 0 10	2 0 5	1.2711	1.2712	3
8 7 4		1.8998	1.9002	1	16 8 2	2 1 1	1.2568	1.2571	5
8 0 10	1 0 5	1.6852	1.6852	7	8 8 12	1 1 6	1.2439	1.2440	3
8 8 6	1 1 3	1.6637	1.6633	18	16 8 4	2 1 2	1.2269	1.2269	4

Note. Miller indices given for the fundamental structure cell $(hkl)_f$ and superstructure cell $(hkl)_{sup}$.

c and cell volume decrease with increasing $PrO_{11/6}$ content, while *a* remains nearly unchanged. A possible explanation of this result is given below: the structure of solid solution α is similar to that of $Bi_{0.7}La_{0.3}O_{1.5}$ reported by Mercurio *et al.* (14); that is, hexagonal layers of cation are stacked along the *c* axis. The *a*–*b* plane parameters are mainly determined by the ionic bonding between O and Bi in the 6*c* site, which is less affected by the substitution of Pr^{3+} for Bi^{3+}. On the other hand, the *c* axis is affected by the bond between Bi/Pr in the 3*a* site and O. Since Pr preferentially occupies the 3*a* site and the ionic radius of Pr^{3+} is smaller than that of Bi^{3+}, the *c* axis is strongly influenced by the substitution of Pr^{3+} for Bi^{3+} and decreases with the increase of $PrO_{11/6}$.

Table 2 shows the variation of lattice parameters vs the $PrO_{11/6}$ content in solid solution γ. The lattice parameters *a* and *c* and the cell volume do not show significant changes within experimental error. From Fig. 3 and Table 2, the following inferences can be drawn: the small variation of lattice parameters probably implies that Pr^{3+} is the major state in the two solid solutions, since the ionic radii Pr^{3+} and Bi^{3+} are close. Horyń *et al.* (15) reported that the fundamental valence of Pr for $Bi_3Pr_{5-x}O_{12}$ ($x = 0.7$) with rhombohedral phase is 3.08, which implies that Pr^{3+} is the major state in the compound.

The small difference between the lattice parameters of the samples makes it difficult to determine the solid solution region accurately by exclusively using the lattice parameteric method, so the phase absence method was also used. The solid solution range for solid solution α is $x = 0.1$–0.3 and for solid solution γ is $x = 0.69$–0.72. This result differs from that of Esaka *et al.* (6). They obtained solid solutions α and γ in the compositional range $x = 0.1$–0.35 and $x = 0.4$–0.7, respectively, by sintering the samples at 900–1200°C. In our experiment, the different solid solution range for α and γ phase could be attributed to the low sintering temperature (850°C). On the other hand, based on the diffraction patterns, we infer that the structure of solid solution γ originates from the fcc structure of Pr_6O_{11}; that is, it is a distorted structure derived from the fcc structure via atomic displacement. As shown in Fig. 2, the strong diffraction lines of the γ phase overlap

TABLE 4
Refined Structure Parameters of $Bi_3Pr_7O_y$ and the Sample with $x = 0.75$, and Metal–Oxygen Interatomic Distances (Å)

Pr content	Atom	Position	*X*	*Y*	*Z*	*B* (Å^2)	Occupation	Discrepancy	Bond lengths (Å)
	Bi	3(*a*)	0	0	0	0.5	0.3	$R_p = 9.876\%$	$d_{Bi/Pr-4O} = 2.446$
$x = 0.7$	Pr	3(*a*)	0	0	0	0.5	0.7	$R_{wp} = 12.47\%$	$d_{Bi/Pr-4O} = 2.376$
	O	6(*c*)	0	0	0.251	1.0	0.75	$s = 2.123$	
	Bi	3(*a*)	0	0	0	0.5	0.28	$R_p = 10.46\%$	$d_{Bi/Pr-4O} = 2.425$
$x = 0.75$	Pr	3(*a*)	0	0	0	0.5	0.72	$R_{wp} = 13.27\%$	$d_{Bi/Pr-4O} = 2.375$
	O	6(*c*)	0	0	0.249	1.0	0.75	$s = 2.323$	

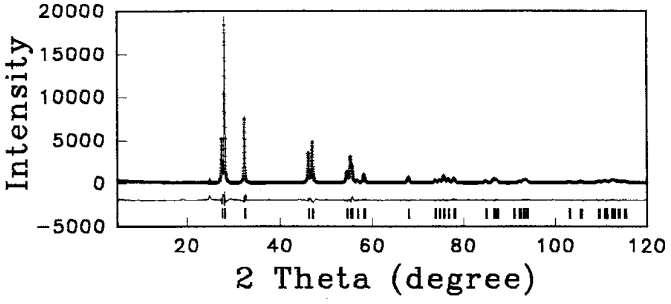

FIG. 4. The result of the Rietveld refinement of the fundamental structure of $Bi_3Pr_7O_y$. (|) denotes peak positions, (+) observed pattern. The calculated pattern overlaps that observed; The difference curve between calculated and observed patterns is shown below.

completely with those of Pr_6O_{11}. For $x = 0.92$–1.0, only Pr_6O_{11}-based solid solution exists. When $x = 0.9$, several small satellites are noted beside the strong diffraction lines, which indicate the presence of subtle distortion. As x decreases, the satellites become stronger and the extent of distortion increases. When $x = 0.69$–0.72, the doublet around $2\theta = 47°$ is of almost identical intensity, which indicates that almost pure solid solution γ is obtained.

The indexing result of $Bi_3Pr_7O_y$ ($x = 0.7$) is listed in Table 3. The calculated spacings d_{cal} coincide well with those observed d_{obs}. The high de Wolff figure of merit, $M = 86$, shows that the result of indexing is reliable. Taking into account strong lines only, the crystal structure of $Bi_3Pr_7O_y$ belongs to the rhombohedral system with lattice parameters $a = 3.8729(5)$ Å and $c = 9.7452(2)$ Å in a hexagonal setting. According to the extinction rule, reflection lines appear only when $h - k + l = 3n$ for index (hkl). It follows that possible space groups are $R\bar{3}m$, $R32$, or $R3m$. The secondary harmonic generator test shows that there is no secondary harmonic signal and that the crystal has a center of symmetry. Therefore, the space group of $Bi_3Pr_7O_y$ is $R\bar{3}m$.

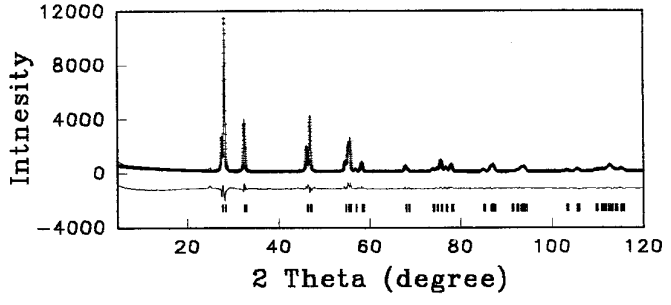

FIG. 5. The result of the Rietveld refinement of the fundamental structure of the two-phase sample with $x = 0.75$ (Pr_6O_{11} and γ phase). (|) denotes peak positions, (+) observed pattern. The calculated pattern overlaps that observed; The difference curve between calculated and observed patterns is shown below.

However, it should be noted that some weak diffraction lines of $Bi_3Pr_7O_y$ could not be indexed for this unit cell. This is possibly due to atomic ordering, which agreed with the results of Wolcyrz *et al.* (15, 16). They observed weak superstructure spots using SAED and HREM, and found the superstructure cell with $a = 8a_0$, $c = 2c_0$ (a_0 and c_0 are the lattice parameters of the fundamental structure) for $BiLa_2O_{4.5}$. We assumed a superstructure cell with $a = 8a_0$ and $c = 2c_0$ ($a_0 = 3.8729$ Å, $c_0 = 9.7452$ Å) and recalculated the d spacings and Miller indices. The indexing result for the superstructure cell is also listed in Table 3. It can be seen that all diffraction lines were indexed, and the result is quite similar to that described by Wolcyrz *et al.* (16).

The results of the Rietveld refinement and interatomic distances of $Bi_3Pr_7O_y$ are presented in Table 4 and graphically shown in Fig. 4. It is seen that the result is reasonable, in spite of the weak diffraction lines. The γ phase crystallizes in the rhombohedral system, and the space group is $R\bar{3}m$. The 3*a* site is occupied statistically by Bi and Pr atoms, the 6*c* sites by statistically distributed oxygen atoms and vacancies. Bi/Pr has eight neighboring oxygen atoms, forming an eightfold coordination cube. This result differs from that of Wolcyrz *et al.* (15, 16). Their result of the refinement of the $BiLa_2O_{4.5}$ structure indicated that its space group was $R3m$, which does not have center of symmetry. Figure 5 shows the result of the Rietveld refinement of the sample with $x = 0.75$. The sample contains two phases: solid solution γ and Pr_6O_{11}-based solid solution. Since the solubility of Bi_2O_3 in Pr_6O_{11} is small, pure Pr_6O_{11} was taken as second phase within first-order approximation. The weight fraction of the second phase is estimated to be about 2.1% from the Rietveld refinement result (17). Based on the lever rule, the right-hand boundary of the γ phase is close to the experimental result using the phase absence method. Interatomic distances of the γ phase in this sample are also listed in Table 4.

$BiO_{3/2}$–$P_{11/6}$–CuO Ternary System

Using phase identification, by means of X-ray powder diffraction analysis of samples with various compositions, the room temperature section of the $BiO_{3/2}$–$PrO_{11/6}$–CuO ternary system was constructed and is shown in Fig. 6. Solid solution Bi_2O_3 was unmarked because of its extremely small solid solution limit (<0.02). In this ternary system, no ternary compound was found. The section at room temperature in $BiO_{3/2}$–$PrO_{11/6}$–CuO can be divided into three two-phase regions and five three-phase regions:

1. $BiO_{3/2}$ + solid solution α + Bi_2CuO_4
2. solid solution α + Bi_2CuO_4+CuO
3. solid solution α + solid solution γ + CuO
4. solid solution γ + Pr_2CuO_4 + CuO
5. Solid solution $PrO_{11/6}$ + solid solution γ + Pr_2CuO_4
6. solid solution α + Bi_2CuO_4

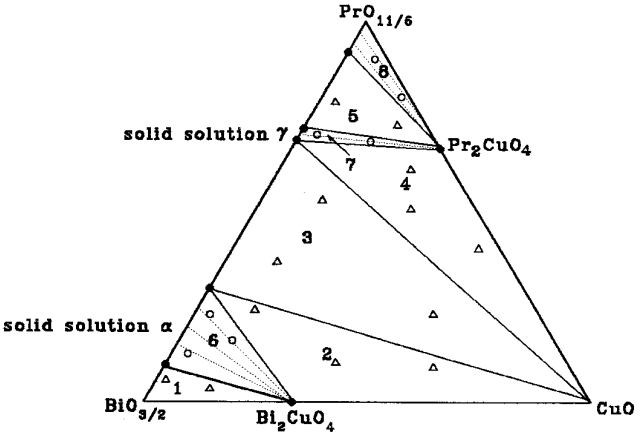

FIG. 6. Subsolidus phase relations in the $BiO_{3/2}$–$PrO_{11/6}$–CuO system. (△) and (◦) denote composition points of three-phase and two-phase regions, respectively.

7. solid solution γ + Pr_2CuO_4
8. solid solution Pr_6O_{11} + Pr_2CuO_4

Webb *et al.* (18) obtained $La_{1-x}Bi_xCuO_3$ for $0.2 \leq x \leq 0.6$ using a high-pressure and high-temperature technique. We failed to synthesize the $BiO_{3/2}$–$PrO_{11/6}$–CuO ternary compound under our experimental conditions. It is expected that the $BiO_{3/2}$–$PrO_{11/6}$–CuO ternary compound can be synthesized under sufficiently high pressure.

ACKNOWLEDGMENTS

This work was supported by the National Natural Science Foundation of China. We thank Professor Wu Bochang for the SHG measurement.

REFERENCES

1. S. A. Hodorowicz *et al., J. Solid State Chem.* **88,** 391 (1990).
2. Boivin *et al., C. R. Seances Acad. Sci. Ser. C* **276,** 1105 (1973).
3. L. S. Sillen and B. Aurivillius, *Z. Cristallogr.* **101,** 483 (1939).
4. J. C. Boivin and D. J. Thomas, *Solid State Ionics* **3/4,** 457 (1981).
5. W. H. Zachariasen, *Acta. Crystallogr.* **4,** 231 (1951).
6. T. Esaka, H. Iwahara, and H. Kunieda, *J. Appl. Electrochem.* **12,** 235 (1982).
7. Ernest M. Levin and Robert S. Roth, *J. Res. Nat. Bur. Stand.* **68,** 197 (1964).
8. H. Iwahara, T. Esaka, and T. Sato, *J. Solid State Chem.* **39,** 173 (1981).
9. T. Takahashi, T. Esaka, and H. Iwahara, *J. Appl. Electrochem.* **5,** 197 (1975).
10. A. Watanabe, *Solid State Ionics* **34,** 35 (1989).
11. A. Watanabe and T. Kikuch, *Solid State Ionics* **21,** 287 (1986).
12. P. Z. Werner, *J. Appl. Crystallogr.* **9,** 216 (1976).
13. P. W. de Wolff, *J. Appl. Crystallogr.* **1,** 108 (1968).
14. D. Mercurio, M. Elfarissi, J. C. Champarnaud-Mesjard, et B. Frit, P. Conflant and et G. Roult, *J. Solid State Chem.* **80,** 133 (1989).
15. R. Horyń, M. Wolcyrz, and A. Wojakowski, *J. Solid State Chem.* **116,** 68 (1995).
16. M. Wolcyrz, L. Kepiński, and R. Horyń, *J. Solid State Chem.* **116,** 72 (1995).
17. D. L. Bish and S. A. Howard, *J. Appl. Crystallogr.* **21,** 86 (1988).
18. A. W. Webb, E. F. Skelton, S. B. Qadri, and E. R. Carpenter, Jr, *J. Solid State Chem.* **102,** 519 (1993).